INTERNATIONAL JOURNAL FOR NUMERICAL METHODS IN FLUIDS
Int. J. Numer. Meth. Fluids 2002; **38**:163–185 (DOI: 10.1002/fld.215)

A method for analysing nesting techniques for the linearized shallow water equations

Yngve Heggelund*,† and Jarle Berntsen

Department of Mathematics, University of Bergen, Norway

SUMMARY

A method for analysing different nesting techniques for the linearized shallow water equations is presented. The problem is formulated as an eigenvector–eigenvalue problem. A necessary condition for stability is that the spectral radius of the propagation matrix is less than or equal to one. Two test cases are presented. The first test case is analysed, and effects of enforcing volume conservation and nudging in time are studied. A nesting technique is found that causes no growth of any eigenvectors for reasonable time steps. This nesting technique is then used on both test cases, and results are compared to an everywhere refined model and a coarse grid model. Copyright © 2002 John Wiley & Sons, Ltd.

KEY WORDS: computational fluid dynamics; nesting; shallow water equations; stability analysis; eigenvalues

1. INTRODUCTION

Oceanic phenomena cover a wide range of spatial scales. To simulate small-scale eddies or the flow around sharp topographic features and submerged installations or discharges of water requires a very fine mesh size. Because of the computational cost it will be prohibitive to cover the whole ocean with this fine mesh size in the foreseeable future. One way of overcoming this difficulty is to build hierarchies of nested models with focus on the area of interest. The success or failure of such efforts will depend both on the qualities of the basic ocean model and on the nesting technique. Conclusions on how nested models perform may depend on the choices of test problems. There is a growing literature describing nested models for the ocean. Major efforts include Spall and Holland [1], Oey *et al.* [2], Fox and Maskell [3, 4], Laugier *et al.* [5, 6], Ginis *et al.* [7], Blayo and Debreu [8], Guillou *et al.* [9] and Rowley and Ginis [10]. Also, experiences from the computational fluid dynamics (CFD) literature on connecting computational sub-domains may be relevant to the ocean model community; see for instance Lien *et al.* [11], Hill and Baskharone [12], Chen *et al.* [13] and Teigland and Eliassen [14].

*Correspondence to: Y. Heggelund, Department of Mathematics, University of Bergen, Norway.
†E-mail: yngve.heggelund@cmr.no

Received February 2000
Revised May 2001

The nesting procedure should preferably conserve fluxes of mass, heat and momentum across the interfaces. In meteorology such a scheme was developed by Kurihara *et al.* [15]. Berger and Leveque [16] have developed general adaptive mesh refinement algorithms for hyperbolic systems that also are conservative across interfaces. Ginis *et al.* [7] applying the technique proposed by Kurihara *et al.* [15] developed a nested primitive equation model that did not fictitiously increase or decrease the transports of mass, momentum and heat through the dynamical interface. Angot and Laugier [17] address the continuity and conservation properties across interfaces. Rowley and Ginis [10] included a mesh movement scheme in the nested ocean model and stated that mass, heat and momentum are conserved during the movement. The model applied in these two studies is based on the reduced gravity assumption so that the deep ocean is at rest below the active upper ocean, and the variables were discretized on non-staggered grids. More general circulation models for the ocean often split the velocity field into external and internal modes and apply different time steps for the two modes. Staggered grids, typically B or C grids [18], are often applied to reduce errors in the phase speeds. This complicates the bookkeeping of fluxes across mesh interfaces, and to our knowledge no nested ocean model based on mode splitting and staggered grids conserve fluxes across mesh interfaces [1–3]. Spall and Holland [1] state that for short time integration this may not be critical whereas for climate studies conservation is most likely to be a critical issue.

Most papers describing nested ocean modelling efforts discuss stability problems and un-smooth solutions across the interfaces. Spall and Holland [1] finding support in Zhang *et al.* [19] state that it may be necessary to sacrifice exact conservation to obtain smooth, stable solutions. To stabilize and smooth the solutions we find that combinations of horizontal and vertical diffusion, filtering the solutions in time and relaxation techniques or nudging are often applied.

In the literature, both one-way and two-way interaction between the coarse and the fine grid have been considered. In a one-way nesting, information is interpolated from the coarse grid to the fine grid, but there is no feedback from the fine grid. Phillips and Shukla [20] argue that a two-way interaction gives a more correct solution on the fine grid and therefore is more favourable. The nesting described in References [1, 2, 7] for instance, is two-way. However, a two-way interaction may introduce instabilities at the interface between the two grids, and such instabilities may severely degrade the solution, see Zhang *et al.* [19]. In some studies data from previously run coarse grid models are used to drive fine grid models, see for instance References [21, 22]. Fox and Maskell [4] compared one-way and two-way nesting and concluded that using the model in one-way nesting mode resulted in more noise at the fine grid mesh boundaries with negligible decrease in computer time.

In order to provide boundary condition for the fine grid, the coarse grid variables must be interpolated to the fine grid. There are numerous techniques that are potentially interesting for performing this task and some of these are considered recently by Alapaty *et al.* [23]. Based on studies with an idealized test case they conclude that zeroth-order interpolation may create large phase errors, quadratic interpolation may create overshooting and they suggest the use of advection equivalent interpolation schemes.

Nested model grids may be adaptive and movable or static. In order to follow evolving oceanic features such as wave fronts and propagating eddies it may be beneficial to apply for instance adaptive mesh refinement methods for hyperbolic systems described by Berger and Oliger [24] or more recently by Berger and Leveque [16]. Blayo and Debreu [8] have recently applied this technique to study the propagation of the barotropic modon and with a

multi-layered quasi-geostrophic model. Rowley and Ginis [10] in their model based on the reduced gravity assumption included a mesh movement scheme. However, as far as we know nested general circulation models with movable meshes have not yet been implemented. To run nested ocean models with large numbers of grid cells on each level is very CPU demanding and to allow the grids to evolve dynamically will add to the computational cost and the complexity of the coding.

Spall and Holland [1] apply the same time step both on the coarse and the fine grid arguing that the coarse grid contributes little to the overall expense and that it would add an additional level of computational complexity for very little gain to have different time steps on the two grid levels. With equal Courant numbers on all levels the quality of the wave propagation relative to the mesh size will be approximately the same, and most of the more recent papers on nesting also refine the time step with the same factor as the spatial resolution, keeping the Courant numbers constant.

A topic for debate in the literature on ocean model nesting is the degree of refinement from one level to the next. Grid ratios from 2:1 to 7:1 have been applied. Spall and Holland [1] conclude that 3:1 and 5:1 ratios perform quite well, and even ratios of 7:1 are able to reproduce the solution reasonably well while the features are mostly contained within the fine region. To apply small ratios like 2:1, which is used for instance in Rowley and Ginis [10], may force us to apply many grid levels before we achieve the resolution we would like to have in a given area. On the other hand, large ratios may cause instabilities and un-smooth solutions across the interfaces.

There are numerous combinations of basic ocean models and nesting techniques that are potentially interesting and evidence on how such combinations perform is gradually growing as they are applied both to idealized test cases and to more realistic oceanic problems. The problems addressed so far range from advection of a simple cone, see Alapaty *et al.* [23], through the barotropic modon and baroclinic vortex suggested by Spall and Holland [1] and applied as a test case in References [5] and [17] for instance, to more realistic problems like the Norwegian Coastal Current described in Reference [2].

The stability properties of numerical methods are often studied with the Fourier or the von Neumann method. This is the approach applied in Povitsky and Wolfshtein [25] where a multi-domain method for the solution of elliptic CFD problems is described and analysed. Effects of the internal boundaries are included in the analysis. Their study is for a single linear equation and constant coefficients. The insight by von Neumann analysis is important, but it is difficult or impossible to extend this method to, for instance, the shallow water equations with variable topography or variable Coriolis parameter.

To complement the experiences gained through numerical experiments and von Neumann analysis, a method for analysing nesting techniques based on studying the properties of the propagation matrices is suggested. Let $\bar{U}^n$ be the complete state vector at time level n. A method for estimating the state at level step $n+1$ may then be described

$$\bar{U}^{n+1} = G(\bar{U}^n)\bar{U}^n$$

where $G(\bar{U}^n)$ is the propagation matrix. For real ocean models the length of state vectors makes it infeasible to set up the full propagation matrices. However, for simplified equations and very limited numbers of grid points, the propagation matrices may be constructed. For linear equations and with linear methods the matrices will be constant and the stability

properties will depend on the eigenvalues of G. The absolute value of the largest eigenvalue must be less than or equal to 1 to avoid growth.

In this study various techniques for building nested models for the linearized shallow water equations are analysed. It is shown that for the ideal purely hyperbolic case, one-way nesting causes no stability problems as long as the method on each grid level is stable. However, if the solution at the fine grid is fed back to the coarse grid, one may expect a growth in energy unless some stabilizing techniques are applied. In particular, the enforcement of conservation of volume may create instabilities.

Our set of equations represents a hyperbolic system, which implies that the total energy should stay constant in time. A necessary criterion for the stability of the nested model is non-growth of energy. Exact energy conservation for all possible eigenvectors seems to be impossible to achieve in a two-way nested model. Some fine scale waves propagating out from the fine grid may not be represented on the coarse grid. The criterion used here is therefore a weaker one; we accept a nesting algorithm if the total energy is non-growing in time for all possible modes.

Non-growth of energy in this simplified system is a necessary, but not sufficient criterion for non-growth of energy in a nested version of a full ocean model.

The formulation of the problem as an eigenvalue–eigenvector problem, helps us determine exactly what growth rate/damping rate of the energy to expect in a specific nesting procedure, and also which eigenvectors that are most problematic. It is also a way to establish if one can expect growth of energy with a specific nesting scheme without actually having to integrate the model in time.

The method for analysing stability may be extended to include variable coefficients like topography or Coriolis parameter. When including non-linearities, the eigenvalues will become time dependent, but also for this case the method may be used to study how the growth factors develop over time.

A nesting procedure based on the conclusions from the present study has been implemented for the Bergen Ocean Model (BOM) which solves the Reynolds averaged Navier–Stokes equations and applied to the Norwegian Sea with focus on the shelf break; see Heggelund and Berntsen [26].

2. THE BASIC EQUATIONS

The governing equations are the linearized shallow water equations for a flat bottom area (Equations (1)–(3)).

$$\frac{\partial U_A}{\partial t} = -gH\frac{\partial \eta}{\partial x} \tag{1}$$

$$\frac{\partial V_A}{\partial t} = -gH\frac{\partial \eta}{\partial y} \tag{2}$$

$$\frac{\partial \eta}{\partial t} = -\frac{\partial U_A}{\partial x} - \frac{\partial V_A}{\partial y} \tag{3}$$

U_A and V_A are the horizontal transports in the x- and y-direction respectively, η is the surface elevation and H is the constant depth.

This system of equations is discretized in space and time, and integrated in time using the forward–backward method on the C-grid.

The discretized equations can be written as

$$U_{A_{ij}}^{n+1} = U_{A_{ij}}^{n} - \Delta t g H(\eta_{ij}^{n} - \eta_{i-1j}^{n})/\Delta x \tag{4}$$

$$V_{A_{ij}}^{n+1} = V_{A_{ij}}^{n} - \Delta t g H(\eta_{ij}^{n} - \eta_{ij-1}^{n})/\Delta y \tag{5}$$

$$\eta_{ij}^{n+1} = \eta_{ij}^{n} - \Delta t[(U_{A_{i+1j}}^{n+1} - U_{A_{ij}}^{n+1})/\Delta x + (V_{A_{ij+1}}^{n+1} - V_{A_{ij}}^{n+1})/\Delta y] \tag{6}$$

where Δx and Δy are the grid spacings in the x- and y-direction respectively, Δt is the time step, the superscript denotes the time level, and the subscript denotes the grid index.

There is no diffusion or viscosity except for numerical diffusion.

3. THE NESTING PROCEDURE

Figure 1 shows a portion of the nested grid. The grid is staggered, meaning that the velocities are given at cell interfaces and the surface elevation is given at the cell centre. When choosing the grid ratio between the coarse and the fine grid, two conflicting considerations have to be taken into account. With a large grid ratio, much of the fine scale phenomena on the fine grid is not resolvable on the coarse grid. This may cause increased disturbance of signals passing from the fine grid to the coarse grid. On the other hand, a small ratio may force us to apply

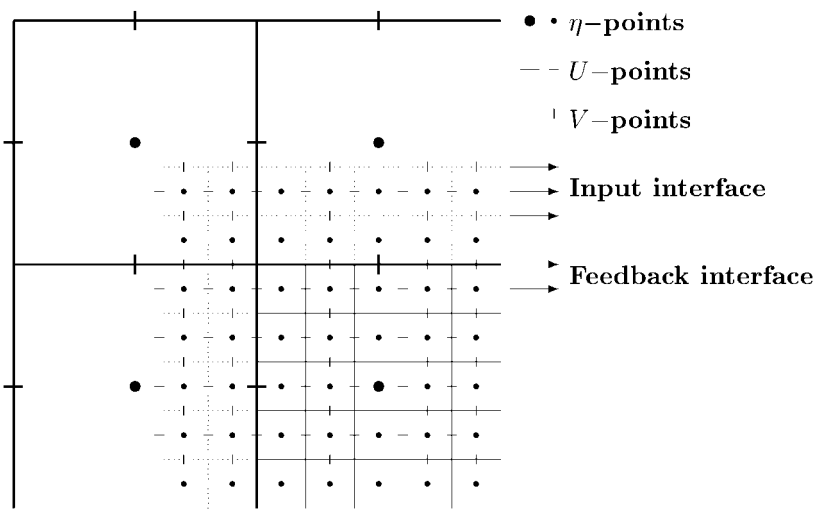

Figure 1. Portion of the nested grid. The coarse grid points are denoted by large symbols, and fine grid points with small symbols.

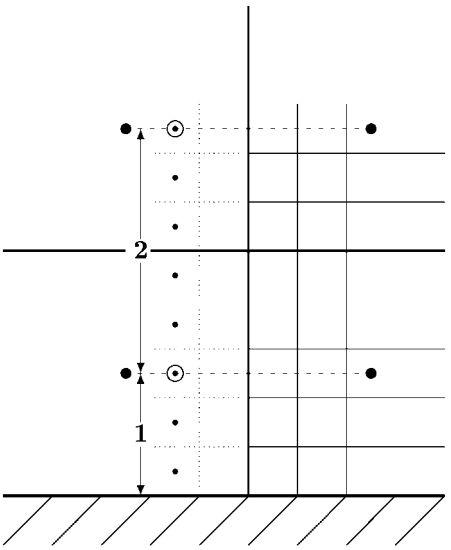

Figure 2. Interpolation of ghost cell η-values. The interpolation method is bilinear interpolation of the four closest coarse grid η-values, except for the ghost cells near boundaries (region marked (1) in the figure), where the value interpolated to the nearest open circle in the figure is used.

many grid levels before achieving a desired resolution in a given area. Based on results from Spall and Holland [1], we have chosen a grid ratio of 5 : 1. The time step on the fine grid model is 1/5 of the time step on the coarse grid model.

Boundary values for the fine grid are interpolated from the coarse grid solution, and are given at the input interface points (see Figure 1). Then the fine grid model is advanced five time steps until reaching the same time level as the coarse grid model. The computed fine grid field values on and inside the feedback interface (see Figure 1) may then be used to update the coarse grid model values.

3.1. Interpolation and restriction operators

The η-values in the ghost cells are found using a bilinear interpolation of the four nearest η-points on the coarse grid. This is illustrated in Figure 2. An exception is made near the solid boundaries (the region marked '1' in Figure 2). Here the value interpolated to the nearest open circle is used, in order to avoid extrapolation and overshooting.

The velocities in the ghost cells are also found using a bilinear interpolation of the four nearest coarse grid velocities. The normal velocities are interpolated both inside and outside of the interpolated η-values. In order to improve the volume conservation in the interpolation step and in order to avoid overshooting, special exceptions are made to the normal velocities near the solid boundary and near corners of the refined region (region '1' and region '3' of Figure 3), where the value interpolated to the nearest open circle is used. For the tangential velocities, see Figure 4, no exceptions are made near solid boundaries or near corners.

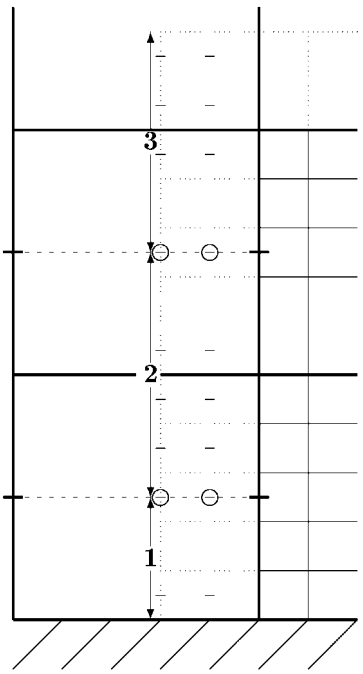

Figure 3. Interpolation of normal velocities. The interpolation method is bilinear interpolation of the four nearest coarse grid U-values. Exceptions are made near the solid boundaries (region '1'), and near the corners of the refined area (region '3'), where the value interpolated into the nearest open circle is used.

The boundary values for η and the velocities in the ghost cells are prescribed before every fine grid time step, overwriting any changes that might have occurred in the fine grid time step.

We have used two different methods for the restriction operator. Common for both methods is that corrections for coarse grid U_A and V_A, are found by five-point averages of the fine point values at the coarse grid interface. One of the methods uses a 25-point average for η, while the other method uses the already restricted U_A and V_A to correct the coarse grid η inside and just outside the nested region. The latter method ensures volume conservation on the coarse grid.

3.2. Energy considerations

The hyperbolic system of equations used in this test case is energy conserving. In the absence of nesting the total energy of the system should therefore stay constant in time.

For long time integrations it is important to conserve volume and momentum, and the nesting should be such that signals may pass through the interface between the two grids without much disturbance. The requirement for the energy is that it should not grow.

The restriction operator used for the velocity does not cause the kinetic energy density to grow. This is because the square of an average value is always smaller than or equal to the

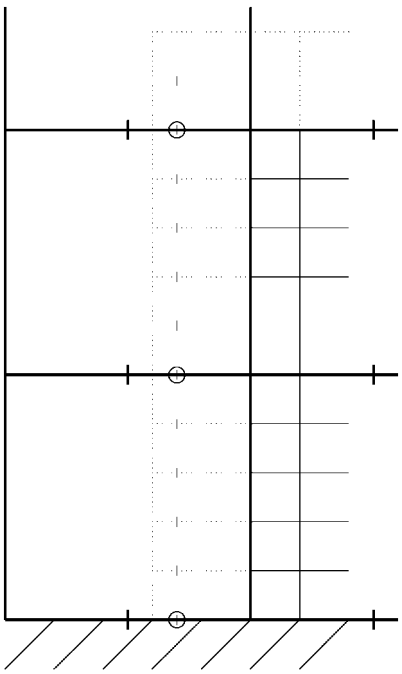

Figure 4. Interpolation of tangential velocities. The interpolation method is bilinear interpolation of the four nearest coarse grid V-values.

average of squared values, see Equation (7).

$$\bar{a} = \frac{a_1 + a_2 + \cdots + a_n}{n}$$
$$\Rightarrow \bar{a}^2 \leqslant \frac{a_1^2 + a_2^2 + \cdots + a_n^2}{n} \tag{7}$$

This means that the restriction operator may reduce, but not increase the kinetic energy when a signal passes the interface from the fine grid area to the coarse grid area. A similar argument holds for the 25-point restriction operator for the surface elevation—it will not cause the potential energy to grow.

Even though the restriction operator and the interpolation operator individually do not cause the energy to grow, a two-way interaction between the grids may still cause growing energy for some modes.

4. STABILITY ANALYSIS OF TEST CASE 1

The first test case has a very simple geometry. The coarse grid model consists of 4×4 grid cells with grid spacings $\Delta X = \Delta Y = 20\,000$ m. The lower right corner of the domain is

refined with a 5×5 mesh (not including ghost cells) with grid spacings $\Delta x = \Delta y = 4000$ m. The equilibrium depth, H, is constant equal to 200 m.

Assume furthermore closed boundaries with no-flow boundary conditions; thus either $U_A = 0$ or $V_A = 0$ at each point on the boundary.

One way of analysing different nesting methods is to set up in detail the propagation matrices for different test cases involving only a limited number of variables. The eigenvalues, eigenvectors and spectral radius for the complete propagation matrices for different nesting techniques may then be computed. A necessary condition for stability of a technique is that the spectral radius is less than or equal to one for the simplified test case. At the same time we want as little damping as possible of at least the longer wave modes through the interfaces between coarse and fine grid.

For test case 1 there are totally 187 wet point variables counting U_A, V_A and η-points on the coarse grid, the fine grid and in the interfaces. We may gather all 187 variables in a 1-D vector W. The method for propagating the solution from coarse time level n to coarse time level $n+1$ may then be written

$$W^{n+1} = GW^n$$

where G is the 187×187 propagation matrix. The matrix G may be constructed by the following algorithm:

Step (i) Forward step in U_A and V_A on the coarse grid:

$$G = I + \Delta t g H A$$

where A is the matrix connecting U_A and V_A on the coarse grid to the η-points on the coarse grid. Matrix elements linking coarse grid U_A-points to the neighbouring η-points are $\pm 1/\Delta x$, $-$ for the east neighbours and $+$ for the west neighbours. Similarly the matrix elements linking coarse grid V_A-point to the neighbouring η-points are $\pm 1/\Delta y$.

Step (ii) Backward step in η on the coarse grid:

$$G = (I + \Delta t B)G$$

where B is the matrix connecting η-points on the coarse grid to U_A and V_A-points on the coarse grid. Matrix elements linking coarse grid η-points to the neighbouring U_A-points are $\pm 1/\Delta x$, $-$ for the east neighbours and $+$ for the west neighbours. Similarly the matrix elements linking coarse grid η-point to the neighbouring V_A-points are $\pm 1/\Delta y$.

Step (iii) Repeat for the fine grid five times:

Interpolate values from the coarse grid to the ghost cells of the fine grid.

$$G = (I + I\mathrm{NEW})G + I\mathrm{OLD}$$

where INEW and IOLD are the matrices coupling coarse grid values to fine grid ghost cells from values at the new and the old time levels respectively. The spatial operations in the interpolation step are as described in Section 3.

Forward step in U_A and V_A on the fine grid.

$$G = \left(I + \frac{\Delta t}{5} g H C\right) G$$

where C is the matrix connecting U_A and V_A on the fine grid to the η-points on the fine grid.

Backward step in η on the fine grid.

$$G = \left(I + \frac{\Delta t}{5} D\right) G$$

where D is the matrix connecting η-points on the fine grid to U_A and V_A-points on the fine grid.

Step (iv) Restriction step: feedback from the fine to the coarse grid

$$G = (I + \mathrm{DRAG} * R)G$$

where I is the identity matrix, R the matrix coupling fine grid values to coarse grid values and DRAG a coefficient defining the strength of the feedback from the fine grid values. The spatial averaging from fine to coarse grid is described in Section 3.

After repeating the steps above the propagation matrix G that brings all variables from time level n to time level $n+1$ is defined, and the LAPACK library [27] is then applied to compute eigenvalues and eigenvectors.

There are infinitely many combinations of methods that are potentially interesting for the sub-steps above that may be analysed. We give some results for seven combinations:

Method 1 No coupling between the two grids.
That is: R is the null matrix in the restriction step and INEW and IOLD null matrices in the interpolation step.

Method 2 One-way nesting.
In the restriction step R is the null matrix and INEW and IOLD are achieved by linear interpolation in time between values of the coarse grid variables at the new and the old time levels.

Method 3 Two-way nesting with averaging of U_A, V_A and η from the fine to the coarse grid.
In the restriction step DRAG is chosen to be one, and INEW and IOLD are achieved by linear interpolation in time between values of the coarse grid variables at the new and the old time levels.

Method 4 Two-way nesting as above, but with a Newtonian feedback from the fine to the coarse grid.
In the restriction step DRAG is chosen to be $DT/900$, that is, the feedback from the fine to the coarse grid is represented by a Newtonian forcing term giving that the coarse grid values overlapping with fine grid values are forced towards averages of the corresponding fine grid values on a time scale of 900 s, see Kurihara and Bender [28].

Method 5 Two-way nesting with averaging of U_A and V_A and enforcing volume conservation.
In the restriction step coarse grid values of U_A and V_A at the interface is computed as averages of the fine grid values. Then the coarse grid values of η at both sides of the interfaces are corrected according to the changes in fluxes across the boundaries due to the corrections in U_A and V_A, see Berger and Leveque [16]. In the restriction step DRAG is chosen to be one, and INEW and IOLD are achieved by linear interpolation in time between values of the coarse grid variables at the new and the old time levels.

Method 6 Two-way nesting as above, but with a Newtonian feedback from the fine to the coarse grid.

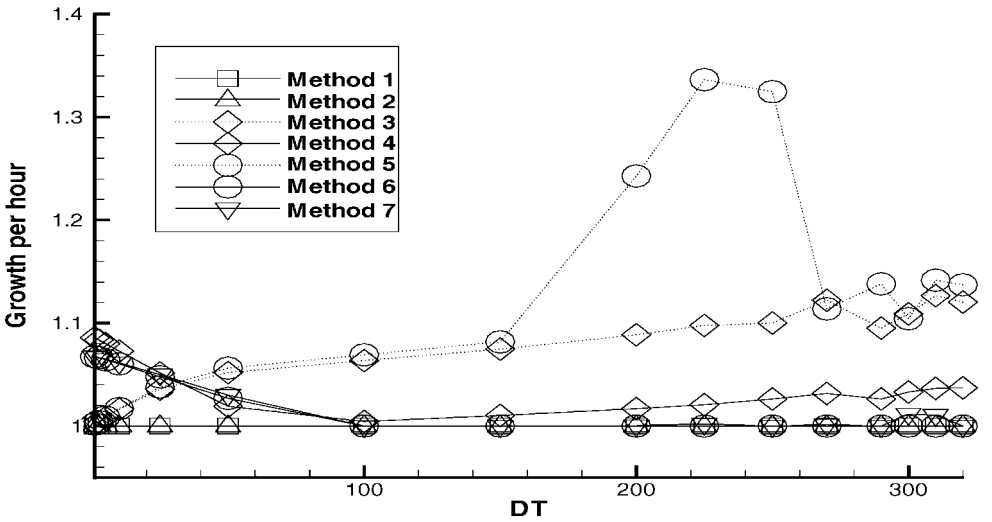

Figure 5. Maximum possible growth over 1 h given by $\rho_{\max}^{3600/DT}$ where $\rho_{\max}$ is the absolute value of the largest eigenvalue. On the horizontal axis values of the time steps in seconds are given.

In the restriction step DRAG is chosen to be $DT/900$, except for this the method is equal to Method 5.

Method 7 As Method 6, but after the feedback step, the surface elevation on the fine grid is corrected uniformly by a constant value in order to achieve global volume conservation.

For each method and for various choices of coarse time steps all eigenvalues of the propagation matrices are computed. The maximum possible growth over 1 h is given by $\rho_{\max}^{3600/DT}$ where $\rho_{\max}$ is the absolute value of the largest eigenvalue. These maximum growth rates are given in Figure 5.

At the coarse grid there are altogether 15 eigenmodes that are possible. We are solving a purely hyperbolic problem and ideally the size of all eigenvalues should be 1. However, including nesting between the grids, we must expect at least some of these modes to die out over time since waves on the fine grid may not be represented on the coarse grid. To study such effects we have computed $\bar{\rho}^{3600/DT}$ where $\bar{\rho}$ is the average value of the absolute values of the 15 largest eigenvalues. The values are given in Figure 6.

From Figures 5 and 6 it is confirmed that with no coupling between the grids (Method 1) there is no growth or damping when using the forward–backward method to solve the linearized shallow water equations without Coriolis term for a flat bottom. The same applies for the one-way nesting case (Method 2). Then the stability of the solution on the coarse grid determines the total stability, and as this solution gets no feedback from the fine grid, it is stable.

Conservation of volume in the restriction step, following the ideas of Berger and Leveque [16] (Method 5), causes an unphysical growth for all reasonable time steps. Zhang *et al.* [19] also point out that it may be necessary to sacrifice conservation between the two grids, and Spall and Holland [1] do not conserve fluxes in their nested ocean model. Fox and Maskell [3] adapt the nesting procedure of Spall and Holland and also sacrifice conservation.

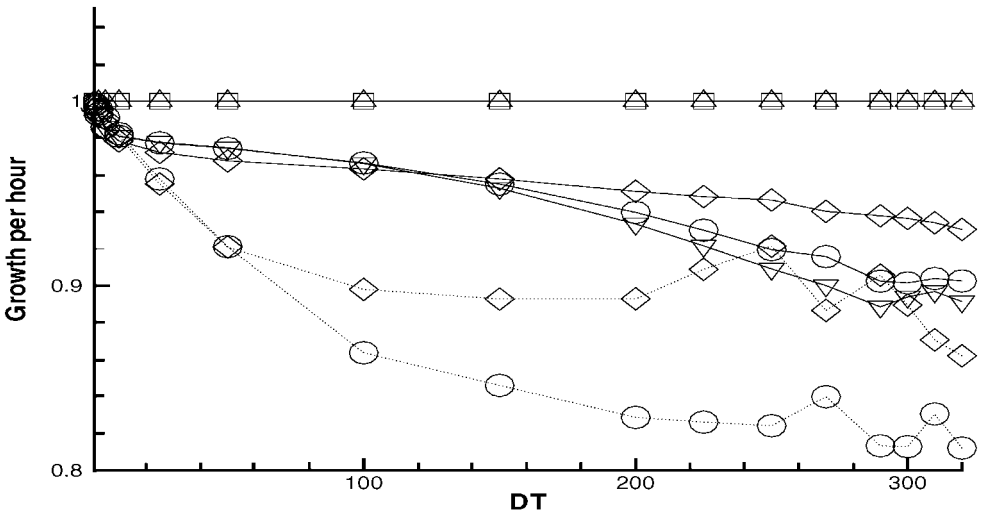

Figure 6. Average growth/damping over 1 h given by $\bar{\rho}^{3600/DT}$ where $\bar{\rho}$ is the average value of the absolute values of the 15 largest eigenvalues. The symbols used for the different methods are as in Figure 5.

They argue that this is not critical in short-term forecasting, but for longer term integrations it will be necessary to conserve fluxes.

Unphysical energy growth may be experienced when using straightforward averaging of fine grid values of U_A, V_A and η in the restriction step (Method 3) without enforcing conservation, but for some unclear reason the growth is less sensitive to the time step than Method 5.

The idea of correcting the solution on the coarse grid using Newtonian forcing (Methods 6 and 7) may stabilize the solution. When using Method 6, there is no growth for time steps larger or equal to 100 s. It is time steps in this range we would like to apply in larger and more realistic experiments. Using a timescale of 900 s for the forcing, we may still experience growth for the smaller time steps, but by modifying this timescale we may avoid this growth.

Correcting the surface elevation in order to achieve global volume conservation (Method 7) seems to destabilize the nesting technique slightly on the larger time steps. This could probably be overcome by adjusting the timescale of the Newtonian forcing, but this has not been explored in this report.

From Figure 6 we notice that for all two-way nested methods the wave modes in average lose energy. For the larger time steps the losses seem to be greater when using Method 5 than Method 3. The losses are considerably reduced when Newtonian forcing is introduced in the restriction step.

Based on the above results, Method 6 seems to be a promising technique. It is stable for all time steps we would like to apply.

Two eigenmodes and their energy development are shown in Figures 7 and 8. Figure 7 shows the most unstable eigenmode for Method 6 with a 10 s time step. The energy grows in accordance with the analysis. Figure 8 shows a stable eigenmode with little damping for Method 6 with a 200 s time step. The energy damping is also here in accordance with the analysis.

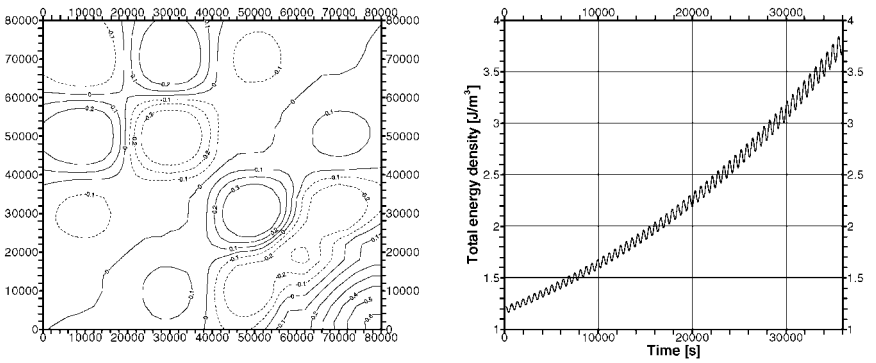

Figure 7. Surface signature and energy development of an unstable mode. The nesting method is Method 6. The timestep is 10 s.

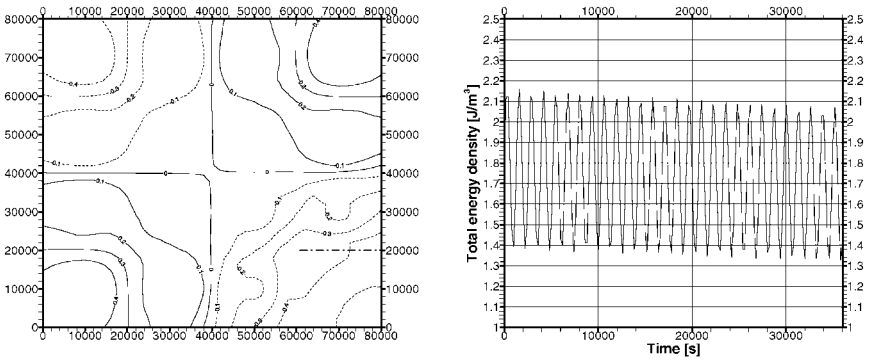

Figure 8. Surface signature and energy development of a stable mode. The nesting method is Method 6. The timestep is 200 s.

5. TEST RUNS

Test runs for the analyzed case and a case with different geometry are presented. The nesting method used is Method 6 from Section 4. The results from the nested case are compared with an everywhere fine grid model and a coarse grid model.

5.1. Test case 1

The field is initialized with $\eta = 1\,\mathrm{m}$ at the lower right coarse grid corner (the whole fine grid mesh) and zero elsewhere. The velocity field is initialized to zero everywhere.

The time step on the coarse grid is set to 180 s, which implies a Courant number Co of

$$Co = \frac{\Delta t}{\Delta x}\sqrt{2gH} \approx 0.56$$

This time step is within the region of stability for Method 6, see Figure 5, so no growth of energy should occur.

Three runs were made. One with the nested model, one with an everywhere fine grid model and one with a strictly coarse grid model. The results are shown in Figure 9.

5.1.1. Comparison of the surface elevation. **Note**: When drawing the contour lines for η, interpolation has to be made on the η-field. In all plots, we have interpolated the field values to a grid with twice the resolution as the fine grid everywhere. The effect of the interpolation can be very clearly seen in the initial structures in Figure 9. The differences seen here are caused purely by interpolations from different data points.

Because of the initial condition, all the plots of surface elevation should be symmetric about the diagonal from the upper left corner to the lower right corner. This is a way to check that the nesting is done symmetrically.

When comparing the nested model with the fine grid everywhere model, the phase speed in the nested model seems to be consistent but not identical to the fine grid model phase speed. After 3600 s of simulation, the two solutions have diverged—probably because of small differences in the phase speed.

Comparison of the nested grid solution to the coarse grid solution, shows that the solutions in the coarse part of the domain are very similar. Some evidence of wave reflection when the disturbance passes from the fine grid to the coarse grid can be seen.

5.1.2. Energy. The total energy density development on the coarse grid and the nested grid is shown in Figure 10. The total energy density is the sum of kinetic and potential energy divided by the total volume. In the coarse grid the energy stays statistically constant. The reason for the fluctuations in the energy is that the solution shifts between the real and imaginary parts of the eigenvectors. The nested model looses total energy as expected. The timescale of the energy loss is, however, much larger than the time it takes for the wave to cross the basin and come back. The timescale of the wave to travel across the basin and come back can be estimated to about 1 h, while the energy has halved in about 10 h.

5.1.3. Volume. The total volume of the water in the coarse grid and the nested grid is shown in Figure 11. This quantity is conserved on the coarse grid with Method 6, but not globally, as this depends on the interpolation operator. Although the volume is oscillating as the signal crosses the interface between the two grids, no long-time growth or decay can occur.

The volume stays at $1.2804 \times 10^{12}\ \mathrm{m}^3 \pm 5 \times 10^7\ \mathrm{m}^3$. With a depth of 200 m, the variation of the volume is on the order of $1/64$ of the volume of a fine grid cell. This small variation was corrected for in Method 7 in Section 4, but it was shown that this correction could give a slight growth of energy when using large time steps.

5.2. Test case 2

In the second test case the coarse grid domain is still 4×4 cells, but the lower left coarse grid cell is removed, and the three coarse grid cells around the removed cell are refined. The field is initialized with $\eta = 1$ m along the upper boundary and zero elsewhere. The velocity field is initialized to zero everywhere. Three runs were made with this test case also; nested grid, everywhere fine grid and everywhere coarse grid.

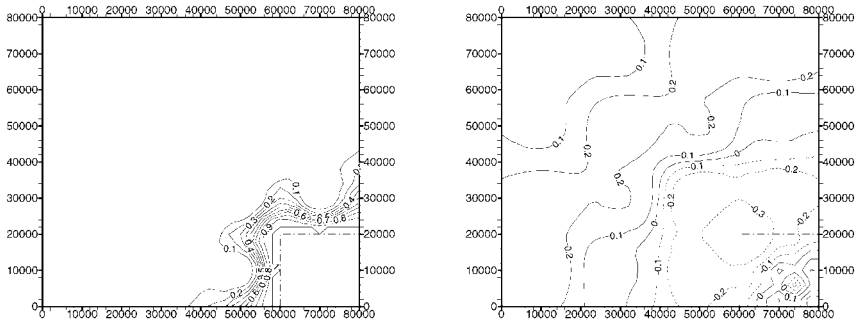

Nested grid. Initially

Nested grid. 1440 s

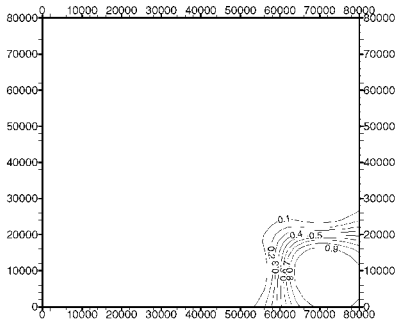

Coarse grid. Initially

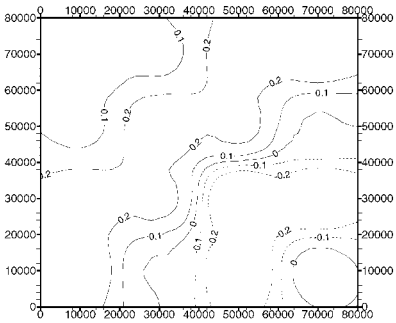

Coarse grid. 1440 s

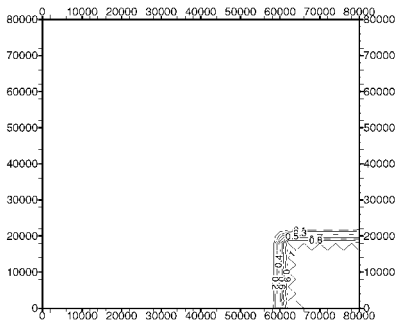

Fine grid. Initially

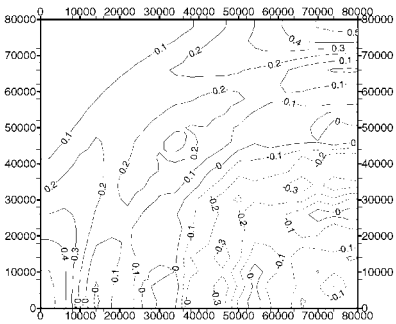

Fine grid. 1440 s

Figure 9. Case 1. Comparison of surface elevation between the nested grid, coarse grid and fine grid models. The boundary of the nested area is shown with the dash–dot lines.

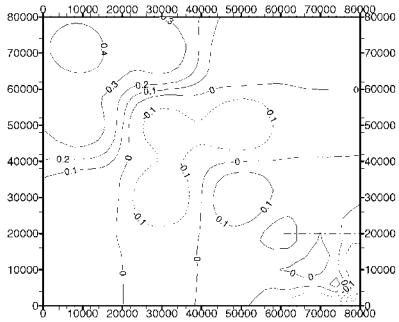

Nested grid. 2160 s

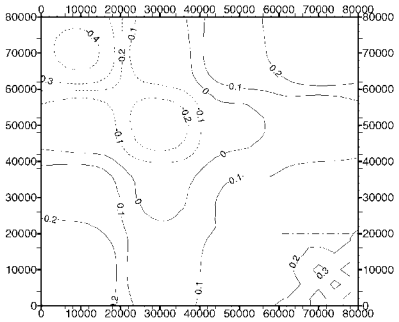

Nested grid. 3600 s

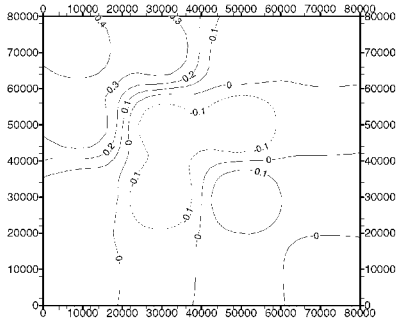

Coarse grid. 2160 s

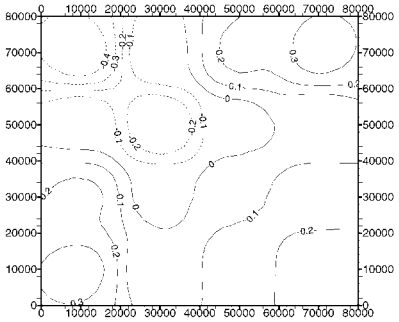

Coarse grid. 3600 s

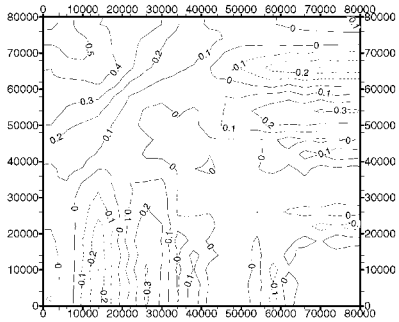

Fine grid. 2160 s

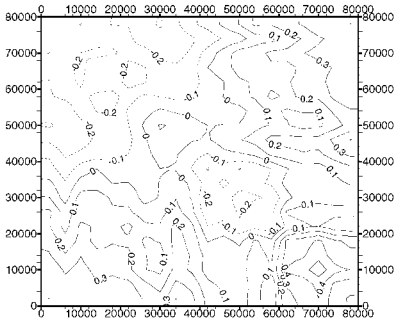

Fine grid. 3600 s

Figure 9. *Continued.*

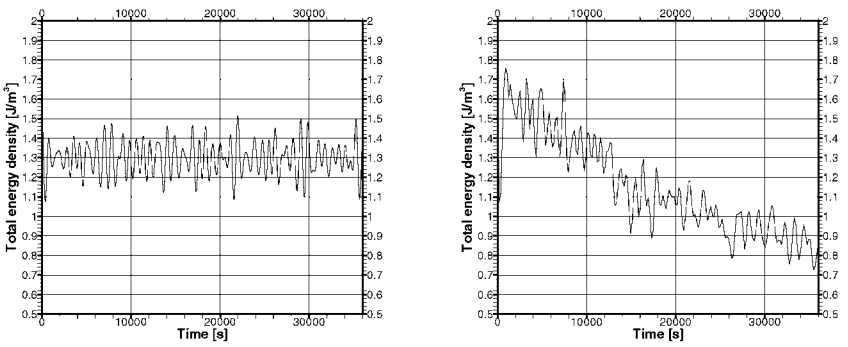

Coarse grid Nested grid

Figure 10. Test Case 1. The total energy development in the coarse grid model and the nested model.

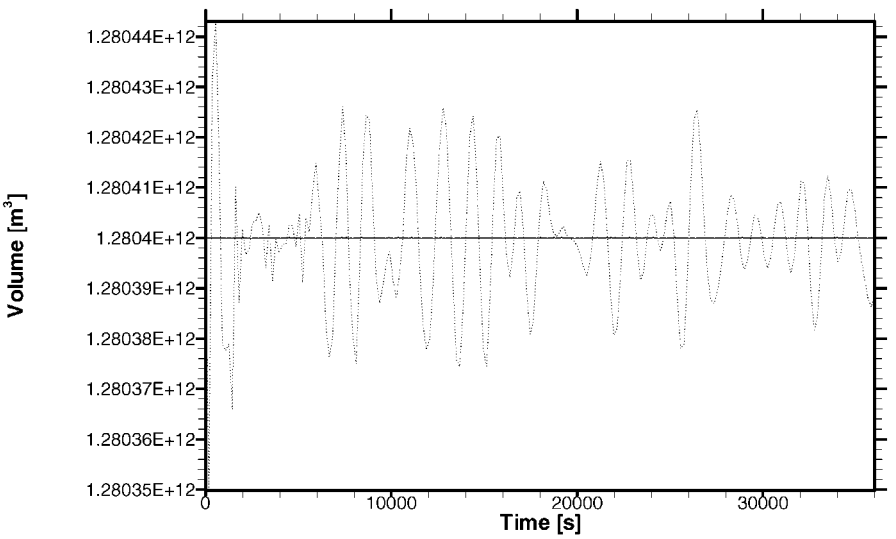

Figure 11. Test Case 1. The total volume development in the coarse grid model (solid line) and the nested grid model (dotted line).

5.2.1. Comparison of surface elevation. The nested model shows less structure on the refined grid than the fine grid everywhere model (Figure 12). This is because the wave front is not well resolved in the coarse grid model, and therefore is not as sharp as the fine grid everywhere model when it enters the nested area. Because of this, these two cases have somewhat different forcing in this area.

Comparison of the nested model to the coarse grid model shows that the coupling from the fine grid area in the nested model can change the solution in the coarse grid part of the nested model area. From the last column in Figure 12, we find that the area with negative

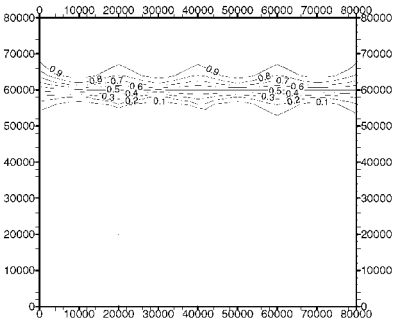

Case 2. Nested grid. Initially

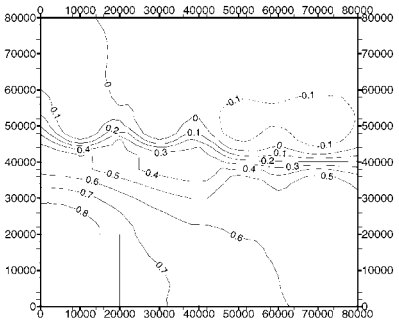

Case 2. Nested grid. 1440 s

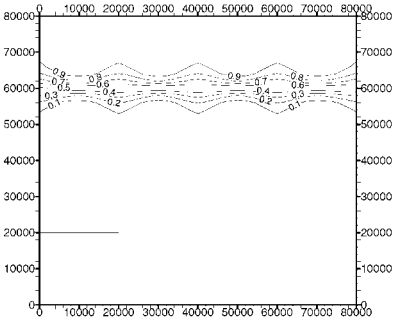

Case 2. Coarse grid. Initially

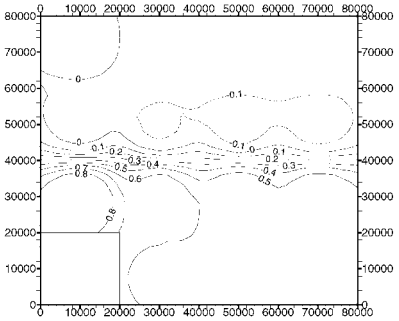

Case 2. Coarse grid. 1440 s

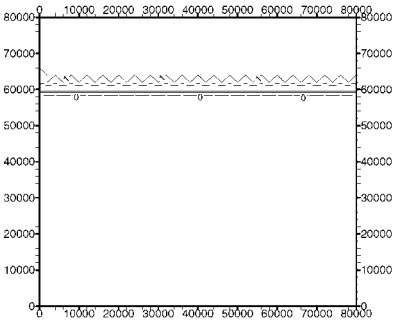

Case 2. Fine grid. Initially

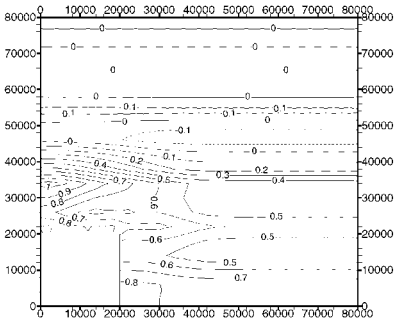

Case 2. Fine grid. 1440 s

Figure 12. Case 2. Comparison of surface elevation between the nested grid, coarse grid and fine grid models. The boundary of the nested area is shown with the dash–dot lines.

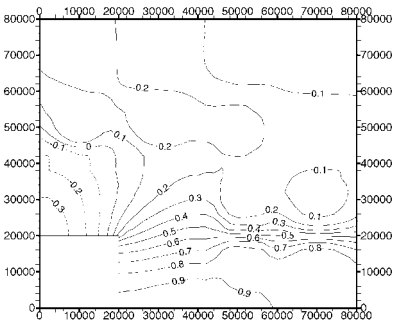

Case 2. Nested grid. 2160 s

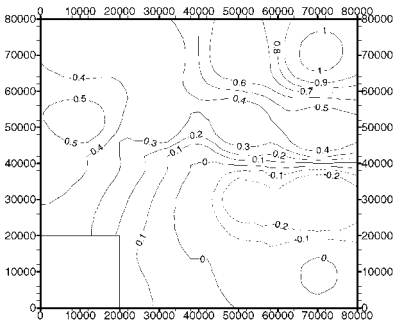

Case 2. Nested grid. 3600 s

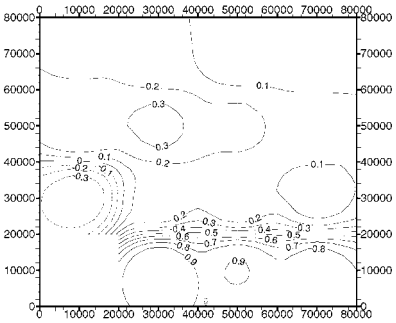

Case 2. Coarse grid. 2160 s

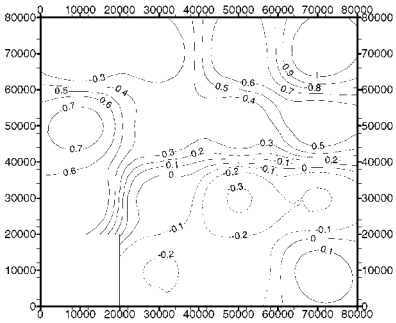

Case 2. Coarse grid. 3600 s

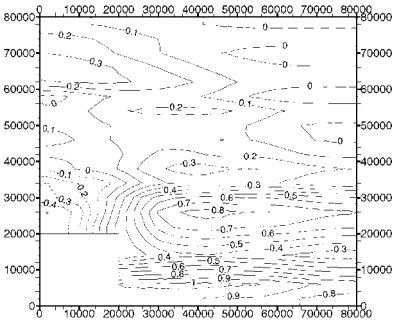

Case 2. Fine grid. 2160 s

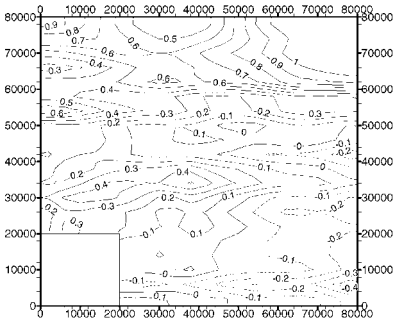

Case 2. Fine grid. 3600 s

Figure 12. *Continued.*

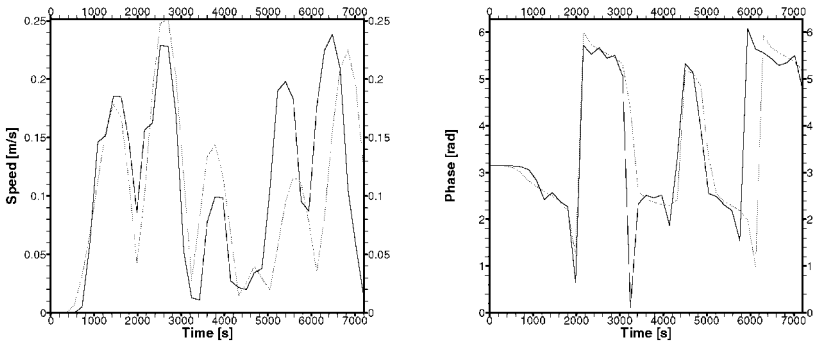

Figure 13. The speed and the phase at the corner of the removed coarse grid cell in the fine grid everywhere model (solid) and the nested model (dotted).

surface elevation in the lower half of the plot is shifted to the right in the nested model, which seems more consistent with the solution on the fine grid everywhere model than the solution on the coarse grid model.

5.2.2. Speed and phase at the corner of the removed cell. As another tool for investigating the effect of the nesting, we study the speed $(=\sqrt{((U_A)/(H))^2 + ((V_A)/(H))^2})$ and the phase of the speed near the upper right corner of the removed coarse grid cell. A phase of 0 or 2π means that the speed is directed northward. A comparison is made in Figure 13, where the speed and phase in the fine grid everywhere model is compared to the speed and phase in the nested model the first 2 h of simulation.

The developments of the speeds and phases are very similar, with somewhat less structure in the nested model. This shows that the nesting technique effectively transports the wave through the interface of the nested area. The amplitude of the speed in the nested model is initially somewhat larger than the fine grid model, but after a while the speed in the nested model is always smaller than the fine grid model.

5.2.3. Energy. The total energy density development on the coarse grid and the nested grid is shown in Figure 14. As in Test Case 1 the nested model looses energy as expected. The timescale of the energy loss compared to the timescale of the wave to travel across the basin and return is about 10:1.

5.2.4. Volume. As in Case 1, the volume in the nested case does not grow or decay on average, see Figure 15. The volume stays at $1.2016 \times 10^{12}\ \mathrm{m}^3 \pm 5 \times 10^7\ \mathrm{m}^3$. The variation equals about 1/64 the volume of a fine grid cell.

6. CONCLUSIONS

In this report, we have described a method for analysing the stability of different nesting techniques for the linearized shallow water equations. The analysis involves constructing the

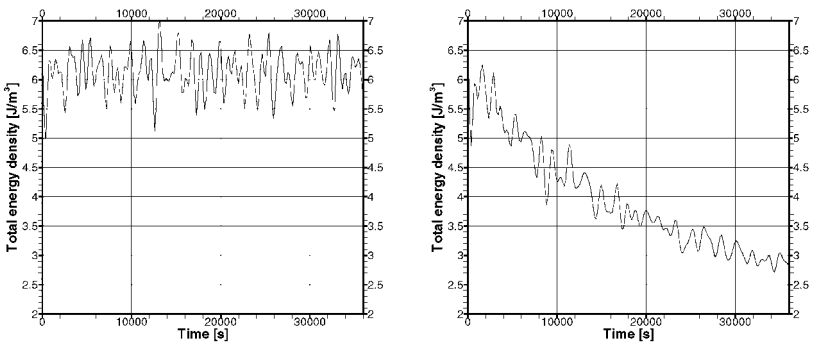

Coarse grid Nested grid

Figure 14. Test Case 2. The total energy development in the coarse grid model and the nested model.

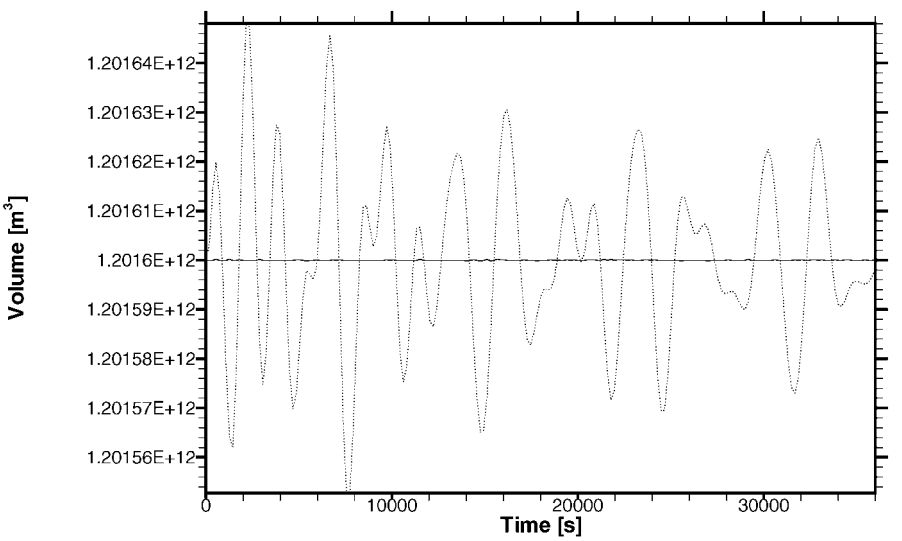

Figure 15. Test Case 2. The total volume development in the coarse grid model (solid line) and the nested grid model (dotted line).

propagation matrix for a particular test case, and calculating its eigenvalues. An eigenvalue greater that one means that the nesting technique is unstable.

Although the analysis is specific to a particular test case, and the propagation matrix has to be constructed again for different test cases, stability for a particular test case is still a necessary condition for stability of test cases with different geometry.

The nesting technique that seems most promising for the analysed test case is implemented for another test case with different geometry. No growth of energy could be seen in this test case either, which indicates that the result may be valid for an even larger class of test cases.

It is demonstrated that methods focusing only on conservation of volume and mass may be unstable. A major finding is that the use of Newtonian forcing in the feedback step from the fine grid to the coarse grid may stabilize the solution. By adjusting the timescale of this forcing, the degree of feedback from the fine grid to the coarse grid may be adjusted. With no feedback (infinite timescale), the solution is stable for all considered time steps, while stronger feedback may destabilize the solution.

Another factor that seems to stabilize the computation when used together with the Newtonian forcing is to correct the surface elevation on the coarse grid in order to achieve volume conservation. Volume conservation on the coarse grid is achieved by this technique.

There is almost an infinite number of nesting techniques that could have been tested. Among the methods tested here, the method based on volume conservation and Newtonian forcing (Method 6), seems to be a promising one. This method is used for two test cases and seems to give reasonable results when the surface elevation is compared to an everywhere refined model and an everywhere coarse grid model.

An advantage with the method of reformulating a given problem to an eigenvalue–eigenvector setting, is that it gives an additional way to check the correctness of the code. Starting with eigenvectors with known growth/damping rate, and demonstrating that the eigenvector indeed grows with the predicted rate is a robust check of the consistency of the coding.

The method described here may be extended to more complex settings. Natural extensions would be to include variable topography and Coriolis force. One could also increase the number of cells in the case to be analysed, but there is an obvious advantage of keeping the number of cells low. More cells will increase the condition number of the matrix, and the accuracy of the eigenvalues will decrease as a result.

ACKNOWLEDGEMENTS

This manuscript was prepared during a stay at Thayer School of Engineering, Dartmouth College, and the hospitality of the staff at Thayer School is greatly appreciated. This research has received support from The Research Council of Norway (Programme for Supercomputing) through a grant of computing time. The authors thank an anonymous reviewer for constructive comments.

REFERENCES

1. Spall MA, Holland WR. A nested primitive equation model for oceanic applications. *Journal of Physical Oceanography* 1991; **21**:205–220.
2. Oey L, Zhang Y-H, Chen P. Simulation of the Norwegian Coastal Current in the vicinity of the Halten Bank: comparison with observations and process study of bank-induced meanders. *Journal of Marine Systems* 1992; **3**:391–416.
3. Fox AD, Maskell SJ. Two-way interactive nesting of primitive equation ocean models with topography. *Journal of Physical Oceanography* 1995; **25**:2977–2996.
4. Fox AD, Maskell SJ. A nested primitive equation model of the Iceland-Fareoe front. *Journal of Geophysical Research* 1996; **101**:18259–18278.
5. Laugier M, Mortier L, Dekeyser I. Un modèle bidomaine aux équations primitives en océanographie physique. *Oceanologica Acta* 1994; **17**:355–367.
6. Laugier M, Angot P, Mortier L. Nested grid methods for an ocean model: A comparative study. *International Journal for Numerical Methods in Fluids* 1996; **23**:1163–1195.
7. Ginis I, Richardson RA, Rothstein LM. Design of a multiply nested primitive equation ocean model. *Monthly Weather Review* 1998; **126**:1054–1079.
8. Blayo E, Debreu L. Adaptive mesh refinement for finite-difference ocean models: First experiments. *Journal of Physical Oceanography* 1999; **29**:1239–1250.

9. Guillou S, Popovics B, Nguyen KD. Numerical simulation of water circulation in marinas of complex geometry by a multi-block technique. In *Coastal Engineering and Marine Developments*, Brebbia CA (ed.). WIT Press: Southampton, 1999.
10. Rowley C, Ginis I. Implementation of a mesh movement scheme in a multiply nested ocean model and its application to air–sea interaction studies. *Monthly Weather Review* 1999; **127**:1879–1896.
11. Lien FS, Chen WL, Leschziner MA. A multiblock implementation of a non-orthogonal, collocated finite volume algorithm for complex turbulent flows. *International Journal for Numerical Methods in Fluids* 1996; **25**: 567–588.
12. Hill DL, Baskharone EA. Development of a multiblock pressure-based algorithm using mixed interpolation for turbulent flows. *International Journal for Numerical Methods in Fluids* 1997; **25**:615–631.
13. Chen WL, Lien FS, Leschziner MA. Local mesh refinement within a multi-bloc structured grid scheme for general flows. *Computer Methods in Applied Mechanics and Engineering* 1997; **144**:327–369.
14. Teigland R, Eliassen I. A multiblock/multilevel mesh refinement procedure for CFD computations. *International Journal for Numerical Methods in Fluids* 2001; **34**: to appear.
15. Kurihara Y, Tripoli GJ, Bender MA. Design of a movable nested-mesh primitive equation model. *Monthly Weather Review* 1979; **107**:239–249.
16. Berger M, Leveque R. Adaptive mesh refinement using wave-propagation algorithms for hyperbolic systems. *SIAM Journal on Numerical Analysis* 1998; **35**:2298–2316.
17. Angot P, Laugier M. The FIC method of conservation connection between nested subdomains for an ocean circulation model. *Comptes Rendus de l'Academie des Sciences Paris* 1994; **319**(Serie II):993–1000.
18. Mesinger F, Arakawa A. *Numerical Methods Used in Atmospheric Models*, vol. 1. WMO/ICSU Joint Organizing Committee, Garp Publication Series No. 17, 1976.
19. Zhang D-L, Chang H-R, Seaman NL, Warner TT, Fritsch JM. A two-way interactive nesting procedure with variable terrain resolution. *Monthly Weather Review* 1986; **114**:1330–1339.
20. Phillips NA, Shukla J. On the strategy of combining coarse and fine grid meshes in numerical weather prediction. *Journal of Applied Meteorology* 1973; **12**:763–770.
21. Svendsen E, Berntsen J, Skogen M, Ådlandsvik B, Martinsen E. Model simulation of the Skagerrak circulation and hydrography during SKAGEX. *Journal of Marine Systems* 1996; **8**:219–236.
22. Berntsen J, Svendsen E. Using the Skagex dataset for evaluation of ocean model skills. *Journal of Marine Systems* 1999; **18**:313–331.
23. Alapaty K, Mathur R, Odman T. Intercomparison of spatial interpolation schemes for use in nested grid models. *Monthly Weather Review* 1998; **126**:243–249.
24. Berger M, Oliger J. Adaptive mesh refinement for hyperbolic partial differential equations. *Journal of Computational Physics* 1984; **53**:484–512.
25. Povitsky A, Wolfshtein M. Multidomain implicit numerical scheme. *International Journal for Numerical Methods in Fluids* 1997; **25**:547–566.
26. Heggelund Y, Berntsen J. A two-way nesting procedure for an ocean model with application to the Norwegian Sea. Technical Report 151, Department of Mathematics, University of Bergen, Norway, 2000.
27. Anderson E, Bai Z, Bischof C, Blackford S, Demmel J, Dongarra J, Du Croz A, Greenbaum J, Hammarling S, McKenney A, Sorensen D. *LAPACK Users' Guide*, *Third Edition*. Society for Industrial and Applied Mathematics, 1999.
28. Kurihara Y, Bender MA. Use of a movable nested-mesh model for tracking a small vortex. *Monthly Weather Review* 1980; **108**:1792–1809.

